L. Ken Lauderbaugh Saunders
Assistant Professor,
Mechanical Engineering,
Penn State Erie,
Erie, PA 16563
Mem. ASME

Craig A. Mauch
Senior Project Engineer,
W. H. Brady Inc.,
Milwaukee, WI 53201
Mem. ASME

An Exit Burr Model for Drilling of Metals

The mechanics of the formation of exit burrs for drilling metals are analyzed. A burr formation model is developed where the material in front of the drill is modeled as an axi-symmetric, circular plate of varying thickness. The drilling thrust forces are distributed as a pressure along the top surface of this plate. The stress state is then calculated. Material removal continues until a failure condition is reached. At the point of failure of the plate the remaining material is bent out to form the burr. The model also includes temperature effects. Experimental verification was conducted on 2024-T351 aluminum and on 7075-T561 aluminum. Two types of drill geometry were considered. The experiments were conducted with feeds from 0.05 to 0.35 mm/rev. The model accurately predicts the experimental data. [DOI: 10.1115/1.1383030]

Introduction

In most metal drilling operations, burrs are formed as the drill exits the workpiece. The presence of these exit burrs requires additional manufacturing steps for disassembly and deburring. These additional steps are typically difficult to automate and are usually performed manually. For precision parts, Gillespie [1] points out that deburring and edge finishing can amount to as much as 30 percent of the cost of the part. These additional deburring steps represent an enormous cost to the manufacture of aircraft where the drilled holes can easily number in the hundreds of thousands per plane.

In spite of the costs associated with burrs and the prevalence of drilling operations, the formation of burrs in drilling has received little research attention. Pande and Relekar [2] empirically investigated the effects of various drilling parameters on burr height and thickness. An interesting result presented in this work was that the exit burr height was minimized at ''medium,'' rather than low feedrates. Pande and Relekar did not explain this paradox but hypothesized that the low feedrates resulted in temperature buildup in the workpiece, which affected the burr formation process. The model presented in this paper is used to discuss Pande and Relekar's hypothesis of temperature effects. More recently, Furness, Wu and Ulsoy [3] studied the effects of drilling parameters on hole quality including burr size.

Some analytical studies have been conducted in an attempt to understand the mechanics of the burr formation process. Gillespie and Blotter [4] identified four burr formation models—Poisson, rollover, tear and cutoff. While they were not specifically addressing drilling, the tear model is most applicable to drilling and is included in the modeling in this paper. Ko and Dornfeld [5] and Chern and Dornfeld [6] furthered the development of burr formation models through examining the mechanism of burr formation in orthogonal cutting using SEM micro-machining tests. The basic premise of these approaches is that at the end of the chip formation, plastic deformation begins, and consists of two components. Plastic shear deformation and plastic bending are responsible for deforming the workpiece until the fracture strain is reached. Upon reaching the fracture strain, the remaining material is removed by fracture and the plastically deformed material becomes the actual burr. However, the cutting speeds in this work were slow enough that the temperature effects of actual cutting operations would not be significant. In addition, the method presented best applies to milling and turning operations where the power force component is perpendicular to the exit surface. In drilling, the power force component is parallel to the exit surface.

In the work presented in this paper, the orthogonal cutting burr formation mechanics of other researchers are extended to the more complex cutting mechanics of drilling operations—including indentation, orthogonal cutting and oblique cutting. The effects of temperature are also included in the model. An objective of this effort was to produce a model that was easy to use. Therefore, wherever possible, only ''handbook'' material properties are required inputs. The model and its experimental verification are also put in the context of results found in the literature.

Exit Burr Height Modeling

The material directly in front of the drill is modeled as an axisymmetric circular plate—the shaded area in Fig. 1. The thrust force is distributed as a pressure, q, on the top surface of the ''plate.''

The thrust force is composed of components from three separate regions of the drill [7,8]. These three regions are shown in Fig. 2. Two force components (two regions) are the result of the chisel edge and the third is the force component from the oblique cutting in the lip region of the drill. The forces generated at the chisel edge are modeled as indentation near the center and orthogonal cutting at the outer edges. The thrust force for the indentation is [7,8]

$$TF1 = \frac{8\tau h(1+\varepsilon)(\sin\gamma)R_a}{\cos\gamma - \sin(\gamma-\varepsilon)} \tag{1}$$

where ε is found from:

$$2\gamma = \varepsilon + \arccos(\tan(\pi/4 - \varepsilon/2)) \tag{2}$$

In Eqs. (1) and (2) 2γ is the drill point angle, τ is the material shear yield stress, h is the depth of indentation and R_a is the distance to the transition point (Point A) between regions 1 and 2 and is given by:

$$R_a = \frac{feed/2}{\tan(90° - \gamma)} \tag{3}$$

Region 2 is modeled as orthogonal cutting. Since the cutting motion has both rotational and feed components, a dynamic rake angle must be defined. Furthermore, since the rotational component of the cutting motion varies with radius, separate dynamic rake angles are defined for 5 differential elements along region 2. The dynamic rake angle can then be defined as: $\alpha_d = \alpha + \mathrm{Tan}^{-1}(feed/2\pi Rci)$, where Rci is the radius to the ith cutting element and α is the rake angle. Then the thrust force for each element can be expressed:

$$Fqi_2 = \frac{tb\tau\sin(\beta - \alpha_d)}{\sin(\phi_M)\cos(\phi_M + \beta - \alpha_d)} \tag{4}$$

and the power force for each element is given by:

Contributed by the Manufacturing Engineering Division for publication in the JOURNAL OF MANUFACTURING SCIENCE AND ENGINEERING. Manuscript received July 1998 revised Sept. 2000. Associate Editor: K. Ehmann.

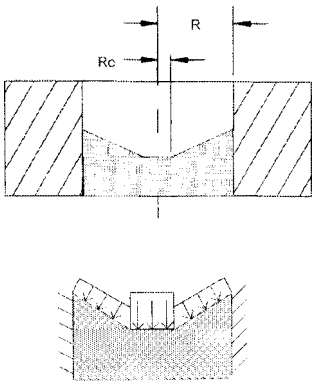

Fig. 1 Burr formation Case I geometry and loading

$$Fpi_2 = \frac{tb\tau\cos(\beta-\alpha_d)}{\sin(\phi_M)\cos(\phi_M+\beta-\alpha_d)} \tag{5}$$

where t=feed/2, $b=(Ro-Ra)/5$, Ro defined in Fig. 1, β =arctan(μ), μ=friction coefficient, ϕ_M is Merchant's shear angle [9]. Then total thrust force and torque for region 2 is:

$$TF2 = \sum_{i=1}^{5} Fqi_2 \tag{6}$$

Then the torque for region 2 can be expressed as:

$$Torque2 = \sum_{i=1}^{5} Fpi_2 * Rci \tag{7}$$

Region 3 is modeled as 50 oblique cutting elements. Each of the 50 elements has different cutting parameters because of the varying geometry and cutting conditions along the lip region. The total thrust force and torque for region 3 can be expressed as:

$$TF3 = 2\sum_{i=1}^{50} Fqi_3 \tag{8}$$

$$Torque3 = 2\sum_{i=1}^{50} Fpi_3 * Ri \tag{9}$$

Fpi_3 and Fqi_3 represent the power and thrust components of each of the 50 elements in region 3 and can be found from the derivation in Mauch and Lauderbaugh [7] and Mauch [8].

To model the burr formation, the thrust force is distributed as a uniform pressure on the top surface of the ''plate.'' The thrust force from the two chisel edge regions are added and distributed as a pressure acting from $r=0$ to $r=Ro$. The thrust force from region 3 is distributed as a second pressure from $r=R_o$ to $r=R$ and the edges of the plate are rigidly constrained (see Fig. 1). Breakthrough and burr formation can then be modeled using two separate conditions.

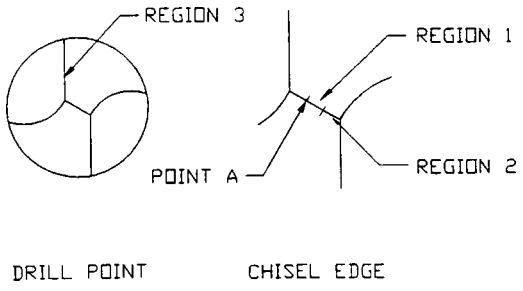

Fig. 2 Three drill tip regions

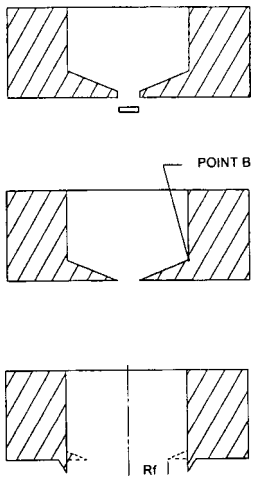

Fig. 3 Burr formation Case II

The first model is designated as Case I. Case I describes the conditions prior to breakthrough, see Fig. 1. As the drilling progresses, the material in front of the drill (the ''plate'' thickness) is reduced, increasing the overall level of stress on the ''plate.'' Von Mises stresses are calculated from this stress state. If the von Mises Stresses exceed the ultimate strength of the material, breakthrough occurs. If not, the drill is advanced half a revolution the stresses recalculated and this process continues until the material in front of the drill fails. At this failure point, the material fractures at some radius, r. At breakthrough, the plate geometry changes and a second plate model is used, Case II, Fig. 3. The material in front of the drill continues to support the thrust force after breakthrough and the cutting continues until the stress at point B reaches the ultimate stress of the material. Once failure at B has occurred, the remaining material is bent over and forms the burr. A detailed model for each case follows.

Case I. The plate model developed for Case I is illustrated in Fig. 1. From Conway [10] the plate equation is:

$$D\frac{d}{dr}\left[\frac{d\phi}{dr}+\frac{\phi}{r}\right]+\frac{dD}{dr}\left[\frac{d\phi}{dr}+\nu\frac{\phi}{r}\right]=-Q \tag{11}$$

where

$$D = Ec^3r^3/12(1-\nu^2) \tag{12}$$

Q=total shear force, ν=Poisson's ratio, E=Young's modulus, c is the slope of the plate thickness and ϕ is the angle of the neutral plane.

However, this equation was developed for a plate with constant slope. For the plate model used in drilling, the height, H, as a function of radius, r, is defined as:

$$H = h_o + U(r-Ro)\left(\frac{h-h_o}{R}\right) \tag{13}$$

where $U=0$ for $r<Ro$ and $U=1$ for $r>Ro$, h_o=the vertical distance from point Ro to the bottom surface of the plate and h =the vertical distance at $r=R$ to the bottom surface of the plate. Then:

$$D = EH^3/12(1-\nu^2) \tag{14}$$

and Eq. (11) yields:

$$KH^3\frac{d^2\phi}{dr^2}+\left[K\frac{H^3}{r}+3KH^2F\right]\frac{d\phi}{dr}+\left[3\nu K\frac{H^2}{r}F-K\frac{H^3}{r^2}\right]\phi=-Q \tag{15}$$

where

$$K=\frac{E}{(12(1-\nu^2))} \quad F=\left[U(r-R_0)\frac{h-h_0}{R}\right]$$

A 2nd order, Euler's method, is used to solve Eq. (15) and the radial and tangential stresses found from:

$$M_r=D\left[\frac{d\phi}{dr}+\upsilon\frac{\phi}{r}\right] \text{ and } \sigma_r=\frac{6M_r}{a^2} \tag{16}$$

$$M_t=D\left[\frac{\phi}{r}+\upsilon\frac{d\phi}{dr}\right] \text{ and } \sigma_t=\frac{6M_t}{a^2} \tag{17}$$

Where a = distance from the neutral plane to the stress element.

The two stresses are then used to calculate a von Mises stress along the bottom surface of the "plate." If the von Mises stress exceeds the ultimate strength then the "plate" is said to fail (breakthrough occurs). If there is no failure, the deflection is calculated and cutter continues to advance and remove an amount of material equal to the thickness of the cut less the deflection. The new thickness is subtracted from the "plate" and a new stress state is calculated. This process is repeated until breakthrough occurs. Once breakthrough occurs, the analysis switches to Case II.

Case II. Equation (11) is again used to model the plate in Fig. 3. However, for Case II, $H=cr$ where c is the slope of the plate. Using Eq. (12), and the transformation $r=e^z$ Eq. (11) can be expressed as

$$\frac{d^2\phi}{dz^2}+3\frac{d\phi}{dz}+(3\nu-1)r\phi=\frac{-16q(1-Ro^2e^{-2z})}{3Ec^3} \tag{18}$$

The solution to Eq. (18) is:

$$\phi=A+\frac{B}{r^3}-\frac{16q}{3Ec^3}\left[\frac{1}{3}\ln r+\frac{Ro^2}{2r^2}\right] \tag{19}$$

$$A=\frac{16q}{3Ec^3}\left[\frac{1}{3}\ln R+\frac{Ro^2}{2R^2}\right]-\frac{B}{R^3} \tag{20}$$

$$B=\frac{16q}{3Ec^3}R^3Ro^2\left[\frac{\frac{1}{3}\ln\frac{Ro}{R}-1.5-\frac{Ro^2}{2R^2}}{-8R^3-Ro^2}\right] \tag{21}$$

The radial and tangential stresses are then found by Eqs. (16) and (17). These stresses are used to calculate a von Mises stress at Point B of the plate shown in Fig. 3. When the von Mises stress at point B is greater than the ultimate strength of the material point B is said to fail and the burr is formed. If failure does not occur, the deflection is found from:

$$w=\int_{Ro}^{R}\phi dr \tag{22}$$

The thickness is reduced by the feed/tooth less the deflection and the process is repeated until failure. At failure, the length of the burr is: $Lburr=R-Rf$, where Rf is the distance shown in Fig. 3.

Temperature Effects

The modeling of the drilling and burr formation process is heavily dependent on material properties, such as yield strength and ultimate strength. These properties are known to vary greatly with increased temperature. Shaw and Cook [11] determined that in metal cutting, strain rate effects offset the temperature effects on yield strength. Therefore, changes in yield strength can be neglected. However, the temperature effects on ultimate strength must be considered.

The temperature model developed describes the temperature on the drilling surface and the propagation of the heat through the workpiece. The temperature of the workpiece at point B is used to determine the reduction in ultimate strength used in determining burr formation.

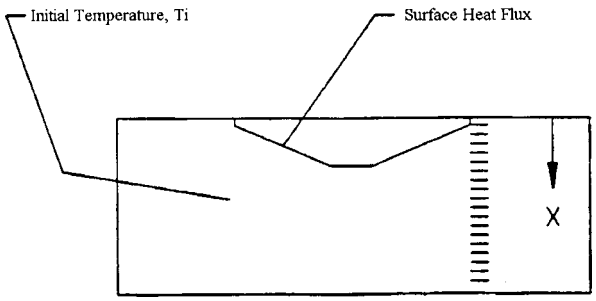

Fig. 4 Heat transfer into the plate

For orthogonal cutting, Trigger and Chao, [12] modeled the heat generated in the shear zone. The temperature, β_s along the shear zone is found by:

$$\theta_s=\theta_0+\frac{A[F_p*V_c(1-B_1)-F_f*V_f]}{J*C_c\rho_c(12V_c)t_{lip}*b_{lip}} \tag{23}$$

A = 0.9 assumed energy appearing as heat in the chip
B_1 = 0.1 heat left in the workpiece
θ_0 = initial workpiece temperature
C_c = specific heat of the chip
ρ_c = density of the chip
J = 1 (Nm/Joule)
F_p = power force component & F_t = feed force component
V_c = cutter velocity & V_f = feed velocity
t_{lip} = chip thickness
b_{lip} = chip width

The model expressed in Eq. (23) describes the conversion of mechanical energy of cutting into heat. Then it is assumed that a portion of the heat, A, is removed with the chip. A similar model can be generated for drilling by assuming that all the work done in cutting is converted to heat and that 10 percent of the heat remains in the workpiece. The heat generated can then be expressed as:

$$\dot{q}=\left(\frac{(\text{Torque})2\pi+(TF)(\text{feed})}{J}\right)\frac{0.1n}{12} \tag{24}$$

"Torque" is the total torque, TF is the total thrust force and n is the speed in rpm. This generated heat is then modeled as a uniform heat flux over the drilling surface (Fig. 4).

Then a 1-D heat transfer model that assumes the heat transfer is perpendicular to the surface with negligible edge effects is used to predict the temperature distribution, Incropera and DeWitt [13]:

$$T(x,t)-Ti=\frac{2q''\left(\frac{\alpha t}{\pi}\right)^{1/2}}{k}\exp\left(\frac{-x^2}{4\alpha t}\right)-\frac{q''x}{k}\text{erfc}\left(\frac{x}{2\sqrt{\alpha t}}\right) \tag{25}$$

Ti = the initial temperature of the plate
q'' = constant heat flux
α = thermal diffusivity
k = thermal conductivity
t = time the q'' has been applied to top surface = 120/rpm
x = distance from the top surface to a point in the plate

The heat flux is applied to the surface of the plate for one half revolution and the temperature distribution is calculated. Then an increment of material is removed, the flux is applied to the new surface and the previous temperature distribution is used to calculate a new distribution.

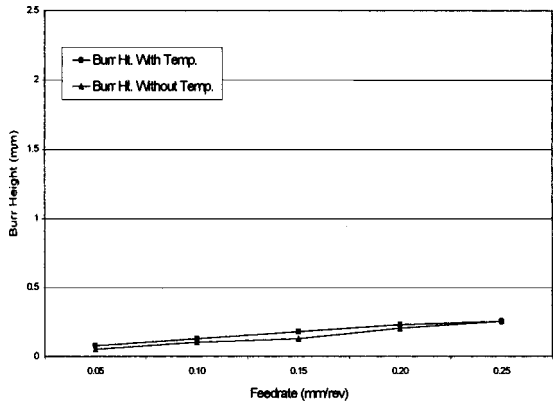

Fig. 5 Burr height with and without temperature

The temperature of the plate at the point where the cutting is occurring is used to reduce the ultimate strength of the material. The reduced ultimate strength causes the material to fail at a larger plate thickness and consequently increases the size of the burr.

Figure 5 shows a comparison of the predicted burr heights with and without temperature effects for 7075 Al with a 4.7625 mm drill. Note that the primary result of the temperature effect is to increase the burr size at low feedrates (below 0.2 mm/rev for this case). At higher feedrates most of the heat generated is removed with the chip before it can propagate into the plate. The most significant effect for this case is at a feed of 0.15 mm/rev.

Experimental System

Experimental verification was performed to validate the simulation model. The drilling was conducted with a pneumatic drill. The work piece was mounted to a force torque dynamometer. After the drilling operation was completed the forces and torques were compared to those predicted by the model. The burr height was then measured and compared to the model predictions.

The pneumatic drill would allow spindle speeds in the range of 300 to 3000 rpm. All the results presented in this paper were at a spindle speed of 1100 rpm. The pneumatic drill was modified so that the feedrate could be varied from 0 to 0.5 mm/rev.

Experimental Results

Two types of aluminum were used in this investigation, 2024-T351 and 7075-T651. Drill sizes were 3.175 mm (1/8 in), 4.7625 mm (3/16 in), 6.35 mm (1/4 in). All drills were 15 cm (6 in) long aircraft drills with 135 deg point angles. Drill tip styles were split point for the 3.175 mm and 4.7625 mm drill and conventional for the 6.35 mm. All drills were high-speed steel with cobalt.

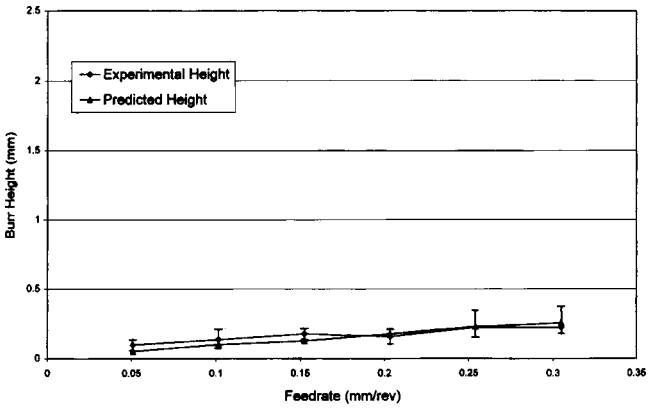

Fig. 6 3.175 mm, 2024-T351

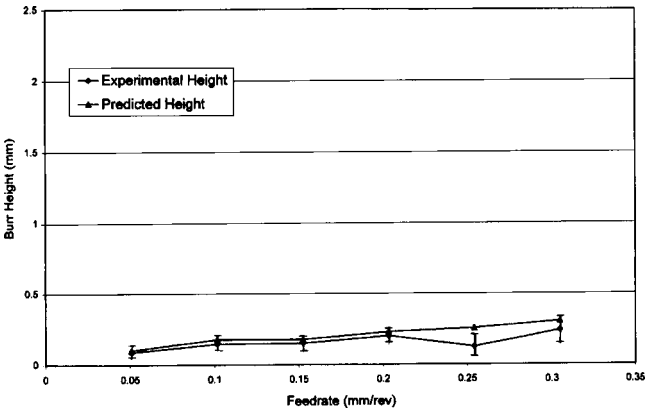

Fig. 7 3.175 mm, 7075-T561

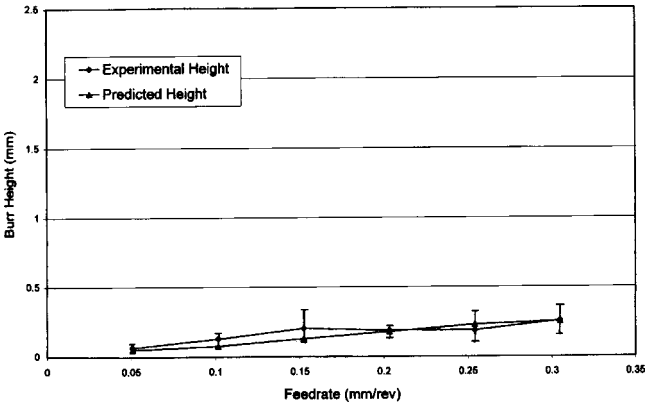

Fig. 8 4.7625 mm, 2024-T351

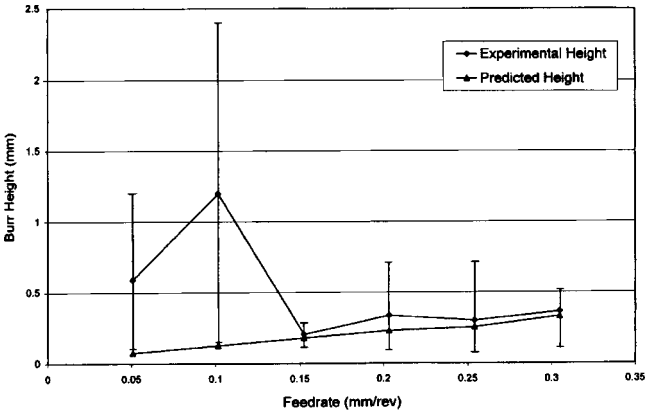

Fig. 9 6.35 mm, 7075-T561

The aluminum plates were 5.3 mm thick. All drilling was done dry with drills in the as sharpened condition. Three holes were drilled with each drill to ''season'' the drill. Feedrates ranged from 0.051 mm/rev (.002 in/rev) to 0.305 mm/rev (.012 in/rev). Five holes were drilled with each drill and the burr heights measured with a tool makers microscope. The results from the five holes were then averaged and plotted with the predicted values in Figs. 6–9. Also shown is the range of the experimental data for each feedrate.

Conclusions

Figures 6 and 7 show the results for the 3.175 mm (1/8 in) split point drill on the two materials. Figures 8 shows the results for the 4.7625 (3/16 in) drill on the 2024 aluminum. The model is doing

an excellent job of predicting the burr size. The predicted values are falling within the range of the experimental values. The model also predicts the overall trend of the data very well.

Split point drills are designed to reduce the thrust force and consequently the burr size. They tend to produce burrs that are evenly distributed around the hole. Figure 9 shows the model predictions and experimental results for a conventional point, 6.35 mm (1/4 in) drill. Here the burr sizes are larger and the model did not agree with the data as well at lower feedrates. However, Fig. 9 also shows the data with error bars showing the range of the 5 measurements at each point. The variability of the data makes it difficult to draw any meaningful conclusion from these results at low feedrates. For the conventional drills, at low feedrates, the burrs tend to be more localized and are produced by tearing, rather than a cutting and bending—typical of the split point case. This tearing burr has a much higher burr height than the nontearing burr. This tearing type burr can also be seen in some of the data for feedrates above 0.2 mm/rev. Here the range is distributed primarily above the average due to a few samples producing a ''tearing'' burr. The model developed here does not attempt to describe the burr formation caused by tearing the annular ring of material to form the burr.

It is interesting to note that the data shown in Fig. 9, indicate that there is an optimal feedrate for minimizing the variation of the burr size—0.15 mm/rev in this case. This feed also results in the minimum burr size based on the experimental data. This indicates that there is an optimum feedrate for minimizing the burr and maximizing the confidence in a burr size prediction.

Prior researchers postulated on the temperature effects on burr size. This model supports their theory that the temperature effects will be greatest at low feedrates. At higher feedrates the thrust force becomes the dominate factor in burr size. However, for the materials and tooling considered in this study the minimum burr occurred at the low feeds, not at the moderate feeds reported.

The model presented describes the mechanism of burr formation in drilling of metals including temperature effects. This model accurately predicts the burr heights for a variety of materials and cutting conditions. This type of model allows researchers to evaluate the trade off between the thrust force increase in burr size with the temperature effects resulting in an optimal feed.

References

[1] Gillespie, L. K., 1979, ''Deburring Precision Miniature Parts,'' Precis. Eng., **1**, No. 4, pp. 189–198.

[2] Pande, S. S., and Relekar, H. P., 1986, ''Investigations on Reducing Burr Formation in Drilling,'' Int. J. Mach. Tool Des. Res., **26**, No. 3, pp. 339–348.

[3] Furness, R. J., Wu, C. L., and Usloy, A. G., 1992, ''Statistical Analysis of The Effects of Feed Speed and Wear on Hole Quality in Drilling,'' *Sensors and Signal Processing for Manufacturing*, S. Y. Liang, C. L. Wu, eds., PED-Vol. 55, pp. 97–112.

[4] Gillespie, L. K., and Blotter, P. T., 1976, ''The Formation Properties of Machining Burrs,'' ASME J. Eng. Ind., **98**, No. 1, pp. 66–74.

[5] Ko, S. L., and Dornfeld, D. A., 1991, ''Mechanics of Deburring and Surface Finishing Processes,'' ASME J. Eng. Mater. Technol., **113**, No. 1, pp. 75–87.

[6] Chern, G. L., and Dornfeld, D. A., 1996, ''Burr/Breakout Model Development and Experimental Verification,'' ASME J. Eng. Mater. Technol., **118**, No. 4, pp. 201–206.

[7] Mauch, C., and Lauderbaugh, L. K., 1990, ''Modeling the Drilling Process—An Analytical Model to Predict Thrust Force and Torque,'' *Computer Modeling and Simulation of Manufacturing Processes*, B. Singh, Y. Im, I. Haque and C. Altan, eds., ASME, New York, pp. 59–66.

[8] Mauch, C., 1990, *Modeling and Control of the Drilling Process to Minimize Exit Burr Height*, Masters Thesis, Rensselaer Polytechnic Institute, Troy, New York.

[9] Merchant, M. E., 1945, ''Basic Mechanisms of the Metal Cutting Process,'' J. Appl. Phys., **16**, pp. 267–275.

[10] Conway, H. D., 1948, ''The Bending of Symmetrically Loaded Circular Plates of Variable Thickness,'' ASME J. Appl. Mech., **16**, pp. 1–6.

[11] Shaw, M. C., and Cook, N. H., 1954, *Metal Cutting Principles*, Third Edition, Massachusetts Institute of Technology, Cambridge, MA, pp. 3.1–3.15.

[12] Trigger, K. J., and Chao, B. T., 1951, ''An Analytical Evaluation of Metal Cutting Temperatures,'' Trans. ASME, **73**, pp. 57–68.

[13] Incropera, F. P., and DeWitt, D. P., 1996, *Fundamentals of Heat and Mass Transfer*, Fourth Edition, John Wiley and Sons, New York.